Transverse-current autocorrelation-function calculations of the shear viscosity for molecular liquids

Bruce J. Palmer
Analytic Sciences Department, Pacific Northwest Laboratory, Richland, Washington 99352
(Received 22 February 1993; revised manuscript received 1 July 1993)

The usual approach to calculating shear viscosities and other thermal transport coefficients from equilibrium molecular-dynamics simulations has been to evaluate the appropriate Green-Kubo relation. An alternative to this method is to examine the long-time behavior of correlations formed from the amplitudes of spontaneous fluctuations in transverse momentum fields (transverse-current autocorrelation functions). For systems in the hydrodynamic limit, long-wavelength fluctuations in transverse momentum fields decay exponentially with a decay constant $1/\tau_H=\mu k^2/\rho$, where k is the wave vector of the fluctuation, μ is the shear viscosity, and ρ is the density. Thus, determination of τ_H leads directly to μ. This approach is used to calculate the shear viscosity for the Lennard-Jones fluid, liquid carbon dioxide, and the TIP4P model of water of Jorgensen *et al.* [J. Chem. Phys. **79**, 926 (1983)].

PACS number(s): 66.20.+d

I. INTRODUCTION

Thermal transport coefficients represent some of the most important properties of liquids; they have, however, remained relatively unexplored in the field of molecular-dynamics simulations. The main obstacle has been the large statistical uncertainties that accompany transport coefficient calculations. Additional complications are associated with the complexity of the autocorrelation functions on which transport coefficient calculations are often based and the issue of finite-size effects. Adequately addressing both the statistical problems and determining the magnitude of finite-size effects usually requires extremely long simulations on a range of system sizes, which has restricted the calculation of thermal transport coefficients primarily to monatomic liquids [1–5]. There have, however, been recent reports in the literature of transport coefficient calculations for molecular liquids using the Green-Kubo relations [6–9].

Much of the work on thermal transport coefficients has focused on the shear viscosity. The most common methods of calculating the shear viscosity are by using the Green-Kubo relations and nonequilibrium molecular dynamics (NEMD). A third approach, which will be the focus of this paper, is the use of transverse-current autocorrelation functions (TCAF's). While the feasibility of using TCAF's to calculate the shear viscosity has been noted, only a few calculations on monatomic liquids have been reported [1,10,11,12]. This paper will investigate the use of TCAF's in calculating the shear viscosity for molecular systems. The TCAF's are easy to calculate and have the advantage of providing insights into finite-size effects due to nonhydrodynamic behavior in the simulation.

The Green-Kubo calculation of the shear viscosity is based on the relation [13,14]

$$\mu=\frac{1}{Vk_BT}\int_0^\infty \langle \mathrm{j}^{xy}(t)\mathrm{j}^{xy}(0)\rangle dt \ , \tag{1.1}$$

where μ is the shear viscosity, V is the volume, T is the temperature, k_B is Boltzmann's constant, and the j^{xy} are the off-diagonal components of the microscopic stress tensor J. For an N-particle system with pairwise additive potentials, the microscopic stress tensor is [14–17]

$$\mathrm{J}=\sum_{i=1}^{N} m_i\mathbf{v}^i\mathbf{v}^i-\tfrac{1}{2}\sum_{i\neq j}^{N}\mathbf{r}^{ij}\nabla\phi_{ij}(r^{ij}) \ , \tag{1.2}$$

where $\mathbf{r}^i$ and $\mathbf{v}^i$ are the coordinates and velocity of particle i, m_i is the particle mass, and $\phi_{ij}(r^{ij})$ is the pairwise interaction potential between particles i and j. The microscopic stress tensor can be calculated as part of the force calculation. However, because there are only three unique off-diagonal components of J, the simulation must be run for long times to get highly converged values for the Green-Kubo integrand over the range of t values which contribute significantly to the integral.

In contrast to equilibrium calculations, NEMD calculations yield only the shear viscosity [18,19]. The NEMD simulation is performed by applying an external force to the system to create either an oscillating or steady-state shear flow. The shear viscosity is calculated from the response of the system to the shearing force. This approach converges more quickly than the equilibrium methods but the additional information available from equilibrium simulations is lost.

Like the Green-Kubo relation, the TCAF calculation described in this paper is also an equilibrium calculation. It therefore requires relatively long simulations. However, the TCAF has two advantages over the Green-Kubo relation. The first is that the nonhydrodynamic behavior in the TCAF's can be easily identified and partially accounted for by some simple generalizations of the hydrodynamic constitutive relations [1,10,20]. The second advantage of TCAF's is that they provide a natural method to estimate the magnitude of finite-size effects. This can be done in a single simulation and the results extrapolat-

ed to the infinite system limit in a straightforward calculation.

The next section provides a brief review of the TCAF and its relationship to the shear viscosity. Some details on calculating the TCAF's from actual molecular-dynamics simulations are given in Sec. III, as well as a description of the nonhydrodynamic corrections to the constitutive relations. The results of calculations on three separate systems are described in Sec. IV. These include the Lennard-Jones fluid, carbon dioxide, and water systems.

II. TRANSVERSE-CURRENT AUTOCORRELATION FUNCTIONS

A heuristic derivation of the connection between hydrodynamics and the transverse-current autocorrelation function is presented in this section [10,21,22]. From hydrodynamics, small-amplitude transverse momentum fields $\mathbf{u}(\mathbf{r})$ of the form

$$\mathbf{u}(\mathbf{r})=(0,u_y(x),0) \tag{2.1}$$

decay according to the diffusion equation

$$\frac{\partial u_y}{\partial t}=\frac{\mu}{\rho}\frac{\partial^2 u_y}{\partial x^2} , \tag{2.2}$$

where μ is the shear viscosity and ρ is the mass density. If a plane-wave initial condition

$$u_y(x,t=0)=u_y^0 e^{ik_x x} \tag{2.3}$$

is assumed for $u_y(x,t)$, then the solution to Eq. (2.2) decays exponentially:

$$u_y(x,t)=u_y^0 e^{-(\mu k_x^2/\rho)t} e^{ik_x x} . \tag{2.4}$$

The decay constant is proportional to the viscosity.

Microscopically, the fluid is composed of discrete particles which are continuously executing random thermal motion, even in equilibrium. At small length scales, momentum gradients appear due to this random motion, and the behavior of these gradients can be analyzed to obtain transport coefficients. A microscopic definition for the transverse momentum fields is

$$u_y^{\text{micro}}(x,t)=\sum_{j=1}^{N} p_y^j(t)\delta(x-x^j(t)) . \tag{2.5}$$

For a periodic system, the delta function appearing in Eq. (2.5) can be expanded in plane waves as

$$\delta(x-x^j(t))=\sum_{k_x}\frac{e^{ik_x[x-x^j(t)]}}{2\pi L} , \tag{2.6}$$

where L is the edge length of the periodic box. Using Eq. (2.6), Eq. (2.5) can be rewritten as

$$u_y^{\text{micro}}(x,t)=\sum_{k_x}\left[\sum_{j=1}^{N} p_y^j(t)e^{-ik_x x^j(t)}\right]\frac{e^{ik_x x}}{2\pi L} . \tag{2.7}$$

Equation (2.7) represents a Fourier expansion of the microscopic momentum field $u_y^{\text{micro}}(x,t)$. The Fourier coefficients $u_y^{\text{micro}}(k_x,t)$ in this expansion are given by

$$u_y^{\text{micro}}(k_x,t)=\sum_{j=1}^{N} p_y^j(t)e^{-ik_x x^j(t)} . \tag{2.8}$$

Equation (2.8) is simply the microscopic definition for the amplitude of a transverse plane-wave momentum field analogous to the initial condition in Eq. (2.3). At times long enough and length scales large enough that hydrodynamics applies, the Fourier coefficients in Eq. (2.7) should also decay exponentially, with the decay constant $\mu k_x^2/\rho$. To extract the long-time decay behavior of $u_y^{\text{micro}}(k_x,t)$, the transverse-current autocorrelation function $C_\perp(k_x,t)$ is formed from the microscopic Fourier coefficients via

$$C_\perp(k_x,t)=\langle u_y^{\text{micro}}(k_x,t)u_y^{\text{micro}}(k_x,0)\rangle , \tag{2.9}$$

where the angular brackets indicate an equilibrium average over initial conditions. If k_x is sufficiently small and t is sufficiently large that hydrodynamics applies, then $C_\perp(k_x,t)$ should decay as

$$C_\perp(k_x,t)\sim e^{-(\mu k_x^2/\rho)t} . \tag{2.10}$$

The TCAF is readily calculated from a simulation using standard techniques. The shear viscosity can, in principle, be extracted from $C_\perp(k_x,t)$ by fitting $C_\perp(k_x,t)$ to an exponential decay at long times and calculating the shear viscosity from the decay constant. The parameters k_x and ρ are already known, so μ follows directly.

A more formal analysis based on linear-response theory [13,22] leads to the relation

$$\chi_\perp(\mathbf{k},\omega)=\frac{\mu k^2\omega}{\omega^2+(\mu k^2/\rho)^2} , \tag{2.11}$$

where $\chi_\perp(\mathbf{k},\omega)$ is the wave-vector- and frequency-dependent susceptibility for transverse momentum disturbances. The frequency is defined from the Fourier transform

$$f(\omega)=\int_{-\infty}^{\infty} dt\, e^{i\omega t}f(t) .$$

Formula (2.11) is true only in the limit of small $\mathbf{k}$ and small ω. The susceptibility can be related to the TCAF using the fluctuation-dissipation theorem, which gives

$$\chi_\perp(\mathbf{k},\omega)=\omega k_B T C_\perp(\mathbf{k},\omega) . \tag{2.12}$$

The Green-Kubo relation results from taking the limit

$$\lim_{\omega\to 0}\lim_{k\to 0}\frac{\omega}{k^2}\chi_\perp(\mathbf{k},\omega)=\mu$$

or, equivalently,

$$\lim_{\omega\to 0}\lim_{k\to 0} k_B T\frac{\omega^2}{k^2}C_\perp(\mathbf{k},\omega)=\mu . \tag{2.13}$$

The Green-Kubo relation is the real-space–real-time representation of Eq. (2.13).

From Eqs. (2.11) and (2.13) the small-k, small-ω behavior of $C_\perp(\mathbf{k},\omega)$ is

$$C_\perp(\mathbf{k},\omega)=\frac{1}{k_B T}\frac{\mu k^2}{\omega^2+(\mu k^2/\rho)^2} . \tag{2.14}$$

Except for the constant of proportionality, this is simply the Fourier transform of Eq. (2.10). Because the Green-Kubo relation assumes that Eq. (2.14) holds, a logical criteria for the validity of the Green-Kubo relation is that the system be large enough to support the behavior indicated in either Eq. (2.14) or Eq. (2.10). Large deviations from a simple exponential decay in $C_\perp(k,t)$ for the smallest values of k accessible in a simulation should be taken as an indication that there may be substantial finite-size corrections to the Green-Kubo value of the shear viscosity.

Computing the TCAF's

To calculate TCAF's in actual practice, it is convenient to use a slightly different form for the Fourier coefficients of the microscopic transverse momentum fields. Instead of Eq. (2.8), the expressions

$$u_\perp^{\text{micro}}(k,t)=\sum_{j=1}^{N}\hat{\mathbf{k}}_\perp\cdot\mathbf{p}^j(t)\sin[\mathbf{k}\cdot\mathbf{r}^j(t)] , \tag{2.15}$$

$$u_\perp^{\text{micro}}(k,t)=\sum_{j=1}^{N}\hat{\mathbf{k}}_\perp\cdot\mathbf{p}^j(t)\cos[\mathbf{k}\cdot\mathbf{r}^j(t)] \tag{2.16}$$

can be used to form the TCAF's. For molecular systems, either the momenta and coordinates of the molecular center of mass of molecule j or the individual atomic momenta and coordinates can be used in these expressions. If a typical distance between an atomic in a molecule and the molecular center of mass is d, then the molecular and atomic definitions of $u_\perp^{\text{micro}}(k,t)$ differ by terms of order dk. The corresponding $C_\perp(k_x,t)$ differ by terms of order d^2k^2, so in the small-k limit both the atomic and molecular definitions give the same $u_\perp^{\text{micro}}(k,t)$ and $C_\perp(k_x,t)$. For finite k, the molecular definition of $u_\perp^{\text{micro}}(k,t)$ appears to give smoother $C_\perp(k_x,t)$ at short times, so the molecular definition of $u_\perp^{\text{micro}}(k,t)$ was used in these calculations.

The vector $\hat{\mathbf{k}}_\perp$ is defined as a unit vector perpendicular to the vector $\mathbf{k}$. For any $\mathbf{k}$, it is possible to construct two orthogonal $\hat{\mathbf{k}}_\perp$'s. The allowable values of $\mathbf{k}$ are

$$\mathbf{k}=\frac{2\pi}{L}(n_1,n_2,n_3) ,$$

where n_1,n_2,n_3 are integers. This paper will follow the crystallographic convention of labeling all equivalent $\mathbf{k}$ vectors by $(|n_1|,|n_2|,|n_3|)$. Note that wave vectors labeled by the same set of indices will correspond to different values of k for different size systems.

For an infinite system, the TCAF should only depend on the magnitude of $\mathbf{k}$. [For finite-size systems, this is not strictly true. The TCAF's for $\mathbf{k}$ vectors that have the same magnitude but are not related by symmetry operations of the periodic lattice may be slightly different. Consider the vectors represented by (2,2,1) and (3,0,0). Both have the same length but cannot be transformed into one another by operations that preserve the symmetry of the lattice.] Furthermore, because of the translational invariance of the system, the TCAF's formed from the sine expansion for $u_\perp^{\text{micro}}(k,t)$ equal the TCAF's formed from the cosine expansion for $u_\perp^{\text{micro}}(k,t)$, so there are a large number of separate contributions to the $C_\perp(k,t)$ for a given value of k. These include all values of $\mathbf{k}$ with magnitude k (however, in this formulation the contribution from $\mathbf{k}$ is equal to the contribution from $-\mathbf{k}$), the sine and cosine formulations of $u_\perp^{\text{micro}}(k,t)$, and the two directions $\hat{\mathbf{k}}_\perp$. For the TCAF formed from the (1,0,0) set of $\mathbf{k}$ vectors, this includes 12 separate contributions to $C_\perp(k,t)$. For optimum statistics, all contributions should be included. The calculations reported here include $C_\perp(k,t)$ for the (1,0,0), (1,1,0), and (1,1,1) vectors.

Once $C_\perp(k,t)$ has been calculated, the shear viscosity can be extracted by fitting $C_\perp(k,t)$ to an exponential decay and using Eq. (2.10) to calculate μ from the decay constant. At short times, however, $C_\perp(k,t)$ is not an exponential function, even in the hydrodynamic limit. This nonexponential behavior can be incorporated phenomenologically using a relaxation-time approximation [10,20] in the constitutive relations for momentum transport. The usual constitutive relation for the diffuse transport of momentum is

$$\mathcal{J}_x^{u_y}=-\frac{\mu}{\rho}\frac{\partial u_y}{\partial x} , \tag{2.17}$$

where $\mathcal{J}_x^{u_y}$ is the x component of the momentum current. This relation can be modified to include short-term memory by writing it as

$$\mathcal{J}_x^{u_y}=-\frac{\mu}{\rho}\int_0^t dt'\phi(t-t')\frac{\partial u_y}{\partial x} , \tag{2.18}$$

where the memory kernel $\phi(t-t')$ is given by

$$\phi(t-t')=\frac{1}{\tau}e^{-(t-t')/\tau} . \tag{2.19}$$

The variable τ is a microscopic relaxation time. Instead of the diffusion equations (2.2), u_y now satisfies the equation

$$\frac{\partial u_y}{\partial t}=\frac{\mu}{\rho}\int_0^t dt'\phi(t-t')\frac{\partial^2 u_y}{\partial x^2} . \tag{2.20}$$

Equation (2.20) can still be solved in a straightforward way for plane-wave initial conditions by using Laplace transforms. If $C_\perp(k,t)$ is normalized to 1 at $t=0$, then the TCAF's decay according to [10,11]

$$C_\perp(k,t)=\frac{1}{2}\left[1-\frac{1}{\Omega}\right]\exp\left[-\frac{(1+\Omega)t}{2\tau}\right]+\frac{1}{2}\left[1+\frac{1}{\Omega}\right]\exp\left[-\frac{(1-\Omega)t}{2\tau}\right] , \tag{2.21}$$

where

$$\Omega=\sqrt{1-4\tau(\mu/\rho)k^2} . \tag{2.22}$$

The simulation curves in this paper were all fitted to Eq. (2.21) to obtain values for μ and τ. Note that for small values of k, Eq. (2.21) reduces to Eq. (2.10). For large

values of k, Ω becomes imaginary, so instead of a monotonic decay, $C_\perp(k,t)$ has a damped oscillatory behavior.

Even with Eq. (2.21) care must be taken to check for nonhydrodynamic behavior. This can manifest itself in two ways. The most obvious indication that the hydrodynamic limit has not been reached is an inability to obtain a good fit using Eq. (2.21) over the entire time interval in which $C_\perp(k,t)$ is calculated. Even when good fits are obtained, the calculated values of μ may show some dependence on k for the smallest available values of k. If the system is large enough to be close to the hydrodynamic limit, then it is possible to correct for the k dependence of μ. Because inversion is a symmetry of the system, $\mu(k)$ must be an even function of k. To order k^2, this implies that

$$\mu(k)=\mu_\infty+ak^2 , \tag{2.23}$$

where μ_∞ is the infinite system limit of μ. Assuming k is small, $\mu(k)$ can be fitted to Eq. (2.23) and the $k\rightarrow 0$ limit taken to obtain μ_∞.

Another source of size dependence in the simulations is the actual size of the system in which the $C_\perp(k,t)$ are calculated. For a given value of k, $C_\perp(k,t)$ could be calculated in systems of dimension $L=2\pi/k$, $4\pi/k$, etc. For the smaller values of L, and k sufficiently large, there could be a difference between $C_\perp(k,t)$ calculated in a cell of size L^3 and $C_\perp(k,t)$ calculated in the $L\rightarrow\infty$ limit. An alternative manifestation of this type of size dependence would be if the $\mu(k)$ calculated from different size simulations lay on different curves. Within the uncertainty in the results, there is no indication that any of the systems investigated here show a significant size dependence of this type.

III. RESULTS

The results of simulations on the Lennard-Jones fluid, carbon dioxide, and water are reported. The simulations were all performed at constant energy using the velocity Verlet algorithm recast as a predictor-corrector [19]. The molecular systems were treated as rigid molecules and the internal constraints were maintained using a variant of the SHAKE algorithm [23,24]. The standard truncated potential

$$\phi(r)=4\epsilon\left[\left[\frac{\sigma}{r}\right]^{12}-\left[\frac{\sigma}{r}\right]^{6}\right]+\phi_0$$

was used for the Lennard-Jones fluid, where ϵ is the well depth and σ is the hard-sphere radius. The constant ϕ_0 is chosen so that the potential vanishes at the cutoff distance r_c. The potentials for carbon dioxide and water both consist of pairwise additive terms $\phi_{ij}(r_{ij})$ which are formed from Lennard-Jones functions and Coulomb interactions. The $\phi_{ij}(r_{ij})$ were truncated by adding terms of the form

$$a_{ij}+b_{ij}(r_{ij}-r_c)$$

and choosing a_{ij} and b_{ij} so that both $\phi_{ij}(r_{ij})$ and its derivative with respect to r_{ij} vanished at the cutoff distance. For the Lennard-Jones fluid, the cutoff was set at $r_c=2.5\sigma$; for carbon dioxide and water, the cutoff was set at $r_c=9.5$ Å.

The TCAF's were calculated from constant-energy simulations. The energy was adjusted until the average temperature matched the target temperature. For most of the individual simulations, the average temperature was within 2 K of the target temperature (the only exception was one of the 500-molecule simulations of carbon dioxide). The time step for the water and carbon dioxide simulations was 2.5 fs; for the Lennard-Jones fluid it was 0.0047 in reduced time units, where $t^*=t/\sqrt{m\sigma^2/\epsilon}$ for a particle of mass m.

Several separate simulations were run for each system. Within each simulation, the individual $C_\perp(k,t)$ were calculated using multiple time origins separated by 0.01 ps (0.0235 in reduced units for the Lennard-Jones fluid). The individual contributions to the TCAF's were combined at the end of each simulation to give an average TCAF for the simulation. For each simulation, the TCAF's were computed for the **k** vectors (1,0,0), (1,1,0), and (1,1,1). For each fluid, simulations on two different size systems were performed. These provided the TCAF's for a total of six different values of k for each fluid.

The curve fits to Eq. (2.21) were done by minimizing the objective function [25]

$$\chi(\tau,\mu)=\sum_{i=1}^{i_{\max}}\frac{[C_\perp(t_i,\tau,\mu)-C_{\perp i}]^2}{\sigma_i^2} \tag{3.1}$$

with respect to the parameters τ and μ. The t_i are the individual times at which the TCAF's are calculated and $i_{\max}$ is the total number of separate t_i's. The $C_{\perp i}$ are the measured values of the TCAF's at time t_i, and $C_\perp(t_i,\tau,\mu)$ is the form (2.21) written explicitly as a function of its parameters. The σ_i's are the uncertainties in the values of the $C_{\perp i}$. The σ_i's are usually not known so an ansatz for them is required. A common choice is to set the σ_i equal to a constant, independent of t_i. However, for these calculations the σ_i were chosen so that the points calculated at short times were weighted more heavily than the points at longer times. For a fixed-length simulation, the number of separate intervals of length t_i is approximately

$$N_i\sim\frac{1}{t_i} .$$

If these intervals are considered as uncorrelated measurements, then the uncertainty associated with the measured values $C_{\perp i}$ is

$$\sigma_i\sim\frac{1}{\sqrt{N_i}} ,$$

which leads to

$$\sigma_i^2\sim t_i . \tag{3.2}$$

This was the choice adopted in these calculations. Note that it is unnecessary to specify the proportionality constant because it does not change the location of the minima in χ. While this analysis is by no means a rigorous

justification, the choice of Eq. (3.2) does account for the increasing uncertainty in the measured TCAF's at longer times, and also serves to minimize the dependence of the curve fit on the cutoff time. All curve fits were performed on the first 4.0 ps of data ($t^*=1.88$ in reduced units for the Lennard-Jones fluid).

For the Lennard-Jones fluid, the validity of Eq. (3.2) was checked by explicitly calculating the σ_i^2 from the simulation data. For short times ($t_i^*<0.5$), Eq. (3.2) appears to overestimate the uncertainty. At longer times, the σ_i^2 are compatible with the linear dependence in (3.2), but the σ_i^2 do not appear to be converged for moderate to large values of t_i^* ($t_i^*\sim 1-2$). Accurate calculations of σ_i^2 would require considerably longer simulations, making the use of computationally determined σ_i^2 in curve fits unattractive.

A. Lennard-Jones fluid

For comparison with the results of other workers, the TCAF's for the truncated Lennard-Jones fluid were calculated at the state point $\rho^*=0.8442$, $T^*=0.722$, where the asterisk indicates the reduced units $\rho^*=\rho\sigma^3$ and $T^*=Tk_B/\epsilon$. Several groups have reported calculations of the shear viscosity at this state point using the Green-Kubo relation. These results have been collected by Erpenbeck [5] and used to estimate the infinite-system shear viscosity as $\mu^*=3.35\pm0.07$, where $\mu^*=\mu\sigma^2/\sqrt{m\epsilon}$.

Two sets of calculations were performed, one on a system containing 864 particles and the other on a system containing 1372 particles. Four runs of 50 000 steps were done for the 1372-particle system and five runs of 50 000 steps were done for the 864-particle system. The three TCAF's from one of the 1372-particle runs, along with the curve fits to Eq. (2.21), are shown in Fig. 1. For the TCAF corresponding to the wave vector (1,0,0), the fit to Eq. (2.21) is quite good. For the shortest-wavelength TCAF, corresponding to the wave vector (1,1,1), there is a noticable discrepency between the fit and the simulation curve at longer times. The difference is reproducible, although the magnitude of the difference varies from simulation to simulation. The (1,1,1) TCAF is clearly not an exponential decay and is beginning to exhibit nonhydrodynamic behavior, but it is beyond the abilities of the simple relaxation-time approximation to account for all of the nonhydrodynamic corrections.

The values of μ^* calculated from each of the individual curve fits are plotted as a function of $k^*=k\sigma$ in Fig. 2. Within the uncertainties, the values of $\mu^*(k^*)$ for the simulations using 1372 and 864 particles lie along the same curves, indicating that the size dependence of $C_\perp(k^*,t^*)$ is mostly contained in k^* and not in the system size itself. These data points were used to calculate a least-squares fit to Eq. (2.23). The resulting parabola is also shown in Fig. 2. The parameters obtained from the fit are $\mu_\infty^*=3.25\pm0.08$ and $a=-0.55\pm0.11$. The error estimates are obtained from standard regression analysis and represent 95% confidence intervals [26]. The value for μ_∞ reported here compares extremely well with Erpenbeck's estimate, although it is slightly lower than Erpenbeck's value. The difference falls within the uncertainties for the two calculations.

The regression analysis used to obtain the uncertainties assumes that the points in Fig. 2 all represent statistically uncorrelated measurements. Because the individual simulations are much longer than the decay times associated with the TCAF's, the assumption that the $\mu(k)$ obtained from different simulations are independent observations should be valid. What is not clear is whether or not the $\mu(k)$ obtained for different values of k from a single simulation are uncorrelated. For small k, the TCAF's for different $\mathbf{k}$ vectors are independent [10,13,20,22], but at larger k couplings between different fluctuations may become important and introduce systematic errors. Assuming that the $\mu(k)$ for each simulation are completely correlated reduces the number of independent measurements by a factor of 3 and leads to a 25–50 % increase in the uncertainties. The appearance of couplings between different fluctuations at higher k would also create sys-

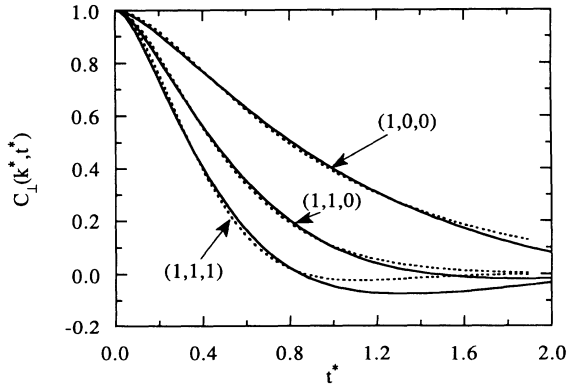

FIG. 1. Transverse-current autocorrelation functions for the Lennard-Jones fluid for the (1,0,0), (1,1,0), and (1,1,1) wave vectors. Time is in reduced units. The solid lines are calculated from a single simulation of 1372 particles; the dotted lines are the curve fits to Eq. (2.21).

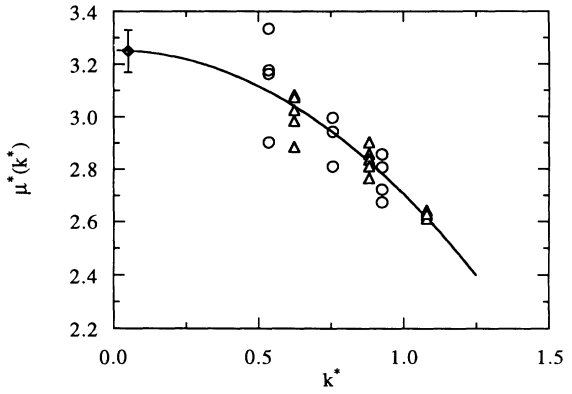

FIG. 2. Viscosity as a function of wave vector for the Lennard-Jones fluid. Both viscosity and wave vector are in reduced units. The circles are calculated from 1372-particle simulations; the triangles are calculated from 864-particle simulations. The solid line is a least-squares fit to Eq. (2.23). The value of μ_∞, along with its uncertainty, is given by the diamond symbol.

tematic errors that would not be reflected in the uncertainties.

B. Liquid carbon dioxide

A modified version [27] of the Murthy-Singer-McDonald (MSM) model for carbon dioxide [28] was chosen for study because previous simulations, using an Ewald summation technique for the long-range forces, indicated that the MSM model successfully reproduces many experimental properties of liquid carbon dioxide, including such dynamical quantities as the orientational relaxation times and the self-diffusion coefficient [24,27]. The truncation used in these calculations changes the pressure substantially, but should not have a large effect on other quantities. Because of the agreement between this model and other experimental properties, it was expected that the shear viscosity would also be close to experiment. Two sets of simulations were done on systems containing 256 and 500 molecules. Six separate simulations were done for the 256-molecule system and four simulations for the 500-molecule system. For both system sizes, each simulation was 50-ps long. The temperature was set at 290 K and the density was set to the liquid saturation density of 0.798 g/cm^3. The shear viscosities derived from the curve fits to the TCAF's are plotted as a function of k in Fig. 3, along with the curve fit to Eq. (2.21).

The viscosities in Fig. 3 are relatively independent of k, although there appears to be a slight increase in μ as k goes to zero. The curve fit to Eq. (2.21) gives the parameters $\mu_\infty = 0.0704 \pm 0.0057$ cP and $a = -0.0516 \pm 0.0621$ cP Å^2. The value of μ_∞ is slightly lower than the experimental value of 0.0790 cP. The values for μ show a large amount of scatter, but within the noise there is no indication that the values of μ obtained from the two different system sizes lie on different curves. The scatter in the data is probably a consequence of the low viscosities and the corresponding long relaxation times for the TCAF's. As a result, there are a relatively low number of uncorrelated intervals in each simulation.

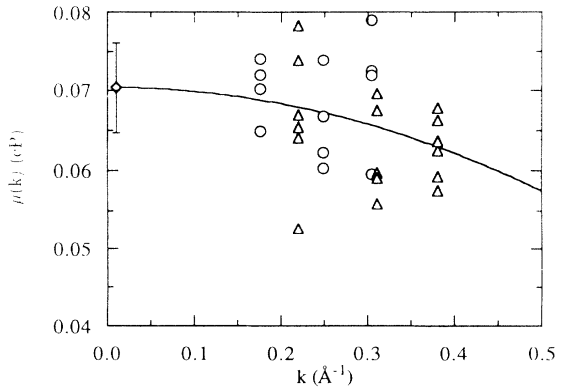

FIG. 3. Viscosity as a function of wave vector for the MSM model of carbon dioxide. The circles are calculated from the 500-molecule simulations; the triangles are calculated from the 256-molecule simulations. The solid line is a least-squares fit to Eq. (2.23). The value of μ_∞, along with its uncertainty, is given by the diamond symbol.

C. TIP4P water

Simulations of TIP4P water [29] were done on systems containing 256 and 500 molecules. Each simulation lasted 50 ps and was performed at the experimental density of 0.997 g/cm^3 for water at 298 K and 1 atm pressure. Four simulations were done for each of the system sizes. The TCAF's from one of the 500-molecule simulations are shown in Fig. 4, along with the curve fits to Eq. (2.21). None of the curves exhibits a monotonic exponential decay and all contain at least one minimum. Furthermore, the curve fits to Eq. (2.21) all display deviations from the simulations at long times, indicating that a significant amount of the nonhydrodynamic behavior is not accounted for by the relaxation-time approximation. There are also some noticeable differences between the curve fit and the simulations at short times.

The inability of Eq. (2.21) to completely capture the behavior of the TCAF's does not appear to result in any obvious pathologies in the behavior of μ as a function of k. The values of μ as a function of k are plotted in Fig. 5 and are consistent with the parabolic form (2.23). Again, the $\mu(k)$ from the two different size simulations appear to lie along the same curves. The parameters derived from a least-squares fit are $\mu_\infty = 0.449 \pm 0.022$ cP and $a = -0.626 \pm 0.122$ cP Å^2. The value of μ_∞ is about half the experimental value of 0.890 cP [30].

The low value of μ_∞ is consistent with the behavior of the diffusion coefficient, which is approximately 50% larger for TIP4P than the experimental value for water. The diffusion coefficient was calculated from the 500-molecule simulations by fitting the mean-square displacement of the oxygen atom to a straight line in the interval between 2.0 and 4.0 ps and using the relation

$$D = \frac{1}{6}\frac{d}{dt}\langle [\mathbf{r}^i(t) - \mathbf{r}^i(0)]^2 \rangle$$

to obtain the diffusion coefficient from the slope. The result was a diffusion coefficient of 3.8×10^{-5} cm^3/s, which is higher than the experimental value of 2.4×10^{-5} cm^2/s [31]. From the theory of Brownian diffusion, the shear

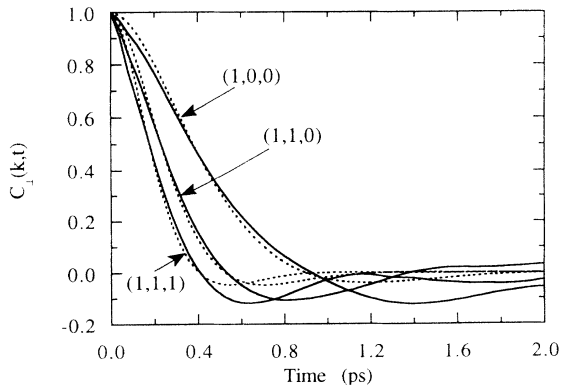

FIG. 4. Transverse-current autocorrelation functions for TIP4P water for the (1,0,0), (1,1,0), and (1,1,1) wave vectors. The solid lines are calculated from a single simulation of 500 water molecules; the dotted lines are the curve fits to Eq. (2.21).

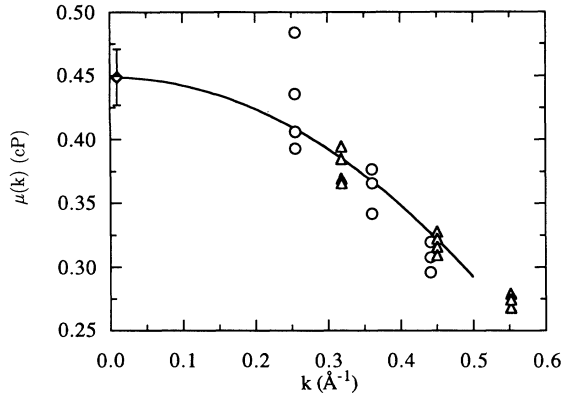

FIG. 5. Viscosity as a function of wave vector for the TIP4P model of water. The circles are calculated from the 500-molecule simulations; the triangles are calculated from the 256-molecule simulations. The solid line is a least-squares fit to Eq. (2.23). The value of μ_∞, along with its uncertainty, is given by the diamond symbol.

viscosity and the diffusion coefficient are approximately inversely related [21], so a qualitative argument can be made that if the diffusion coefficient is too high then the shear viscosity should be too low. This suggests that the extrapolated value of μ is, in fact, close to the actual value of the shear viscosity for TIP4P water.

IV. CONCLUSIONS

The calculations presented here demonstrate that the use of TCAF's represents a viable alternative to the Green-Kubo relations for calculating the shear viscosity from equilibrium molecular-dynamics calculations. Both the Green-Kubo relations and the TCAF's ultimately obtain their information about the shear viscosity from the spontaneous fluctuations in the transverse momentum fields, so it is unlikely that the TCAF's offer substantial advantages over the Green-Kubo relations in terms of statistical reliability. However, the TCAF's do provide greater insight into the contribution of finite-size effects to the calculated value of the shear viscosity. Unlike the Green-Kubo integrand, the expected behavior of the TCAF is known in the hydrodynamic limit. Nonhydrodynamic behavior in the TCAF is easy to identify and gives an immediate indication that the calculated shear viscosity is likely to have a significant size dependence in the range of system size corresponding to the value of k in the TCAF. Even if the Green-Kubo relation is used to obtain the shear viscosity, the simultaneous calculation of the (1,0,0) TCAF would provide an independent assessment of the reliability of the Green-Kubo value.

The k dependence of the shear viscosity can be extracted by calculating the TCAF's for a number of values of k. These can be obtained from a single simulation. The small k behavior of μ is known and can be used to extrapolate μ to the $k \rightarrow 0$ limit. For the Lennard-Jones fluid, this procedure leads to a value of the shear viscosity in agreement with results obtained using the Green-Kubo relation. Unfortunately, for most systems it is unclear *a priori* where the small-k region begins, and this remains the principal difficulty in using the TCAF's as a general tool to calculate the shear viscosity.

The ability to analyze and quantify finite-size contributions to the shear viscosity is an important aspect of shear viscosity calculations. As the calculations on water illustrate, many simulations are likely to fall far short of the hydrodynamic limit, and increasing the simulation size sufficiently to move the simulation into the hydrodynamic limit will require enormous additional effort. The nonhydrodynamic behavior in the TCAF can be partially accounted for by the relaxation-time approximation. Further improvements might be obtained through the use of a more general memory function in the constitutive relation (2.18). The relaxation-time approximation is equivalent to the Maxwell model of a viscoelastic fluid [32], suggesting that the theory of non-Newtonian viscoelastic fluids may provide a rich source of potential constitutive relations. If more of the nonhydrodynamic behavior can be successfully parametrized using a generalized hydrodynamic function, then it would be possible to extract transport coefficients from simulations that are significantly below the hydrodynamic limit. This can result in substantial savings in computer time; a 25% reduction in the system dimension will halve the computer time per time step for a cutoff-based force calculation.

ACKNOWLEDGMENTS

This work was supported by Conservation and Renewable Energy, Office of Industrial Technologies, Advanced Industrial Concepts Program, U.S. Department of Energy. Pacific Northwest Laboratory is operated for the U.S. Department of Energy by Battelle Memorial Institute under Contract No. DE-AC06-76RLO 1830.

[1] C. Hoheisel and R. Vogelsang, Comput. Phys. Rep. **8**, 1 (1988).
[2] B. J. Alder, D. M. Gass, and T. E. Wainwright, J. Chem. Phys. **53**, 3813 (1970).
[3] J. J. Erpenbeck and W. W. Wood, J. Stat. Phys. **24**, 455 (1981).
[4] S. Y. Liem, D. Brown, and J. H. R. Clarke, Phys. Rev. A **45**, 3706 (1992).
[5] J. J. Erpenbeck, Phys. Rev. A **38**, 6255 (1988).
[6] G. Marechal and J.-P. Ryckaert, Chem. Phys. Lett. **101**, 548 (1983).
[7] C. Hoheisel, J. Chem. Phys. **89**, 3195 (1988).
[8] H. Luo and C. Hoheisel, J. Chem. Phys. **94**, 8378 (1991).
[9] H. Luo and C. Hoheisel, J. Chem. Phys. **96**, 3173 (1992).
[10] J. P. Boon and S. Yip, *Molecular Hydrodynamics* (Dover, New York, 1991).
[11] R. Vogelsang and C. Hoheisel, Phys. Rev. A **35**, 1786 (1987).
[12] M. Schoen and C. Hoheisel, Mol. Phys. **65**, 653 (1985).
[13] L. P. Kadanoff and P. C. Martin, Ann. Phys. **24**, 419

(1963).
[14] W. A. Steele, in *Transport Phenomena in Fluids,* edited by H. J. M. Hanley (Marcel Dekker, New York, 1969), Chap. 8.
[15] M. S. Green, J. Chem. Phys. **22**, 398 (1954).
[16] H. Mori, Phys. Rev. **112**, 1829 (1958).
[17] E. Helfand, Phys. Rev. **119**, 1 (1960).
[18] A. W. Lees and S. F. Edwards, J. Phys. C **5**, 1921 (1972).
[19] M. P. Allen and D. J. Tildesley, *Computer Simulation of Liquids* (Clarendon, Oxford, 1987).
[20] D. Forster, *Hydrodynamics, Fluctuations, Broken Symmetry and Correlation Functions* (Benjamin/Cummings, Reading, MA, 1975).
[21] D. A. McQuarrie, *Statistical Mechanics* (Harper & Row, New York, 1976).
[22] J.-P. Hansen and I. R. McDonald, *Theory of Simple Liquids,* 2nd ed. (Academic, London, 1986).
[23] B. J. Palmer, J. Comput. Phys. **104**, 470 (1993).
[24] B. J. Palmer and B. C. Garrett, J. Chem. Phys. **98**, 4047 (1993).
[25] W. H. Press, B. P. Flannery, S. A. Teukolsky, and W. T. Vetterling, *Numerical Recipes* (Cambridge University Press, Cambridge, 1988).
[26] J. Neter, W. Wasserman, and M. H. Kutner, *Applied Linear Statistical Models* (Irwin, Homewood, IL, 1985).
[27] L. C. Geiger, B. Ladanyi, and M. E. Chapin, J. Chem. Phys. **93**, 4533 (1990).
[28] C. S. Murthy, K. Singer, and I. R. McDonald, Mol. Phys. **44**, 135 (1981).
[29] W. L. Jorgensen, J. Chandrasekhar, J. D. Madura, R. W. Impey, and M. L. Klein, J. Chem. Phys. **79**, 926 (1983).
[30] *CRC Handbook of Chemistry and Physics,* 52nd ed., edited by R. C. Weast (Chemical Rubber, Cleveland, 1971).
[31] K. Krynicki, C. D. Green, and D. W. Sawyer, Faraday Discuss. Chem. Soc. **66**, 199 (1978).
[32] R. B. Bird, R. C. Armstrong, and O. Hassager, *Dynamics of Polymeric Liquids* (Wiley, New York, 1977), Vol. 1.